Chromatin accessibility and H3K9me3 landscapes reveal long-term epigenetic effects of fetal-neonatal iron deficiency in rat hippocampus

Shirelle X. Liu[1,2], Aarthi Ramakrishnan[3], Li Shen[3], Jonathan C. Gewirtz[2], Michael K. Georgieff[1] and Phu V. Tran[1*]

Abstract

Background Iron deficiency (ID) during the fetal-neonatal period results in long-term neurodevelopmental impairments associated with pervasive hippocampal gene dysregulation. Prenatal choline supplementation partially normalizes these effects, suggesting an interaction between iron and choline in hippocampal transcriptome regulation. To understand the regulatory mechanisms, we investigated epigenetic marks of genes with altered chromatin accessibility (ATAC-seq) or poised to be repressed (H3K9me3 ChIP-seq) in iron-repleted adult rats having experienced fetal-neonatal ID exposure with or without prenatal choline supplementation.

Results Fetal-neonatal ID was induced by limiting maternal iron intake from gestational day (G) 2 through postnatal day (P) 7. Half of the pregnant dams were given supplemental choline (5.0 g/kg) from G11–18. This resulted in 4 groups at P65 (Iron-sufficient [IS], Formerly Iron-deficient [FID], IS with choline [ISch], and FID with choline [FIDch]). Hippocampi were collected from P65 iron-repleted male offspring and analyzed for chromatin accessibility and H3K9me3 enrichment. 22% and 24% of differentially transcribed genes in FID- and FIDch-groups, respectively, exhibited significant differences in chromatin accessibility, whereas 1.7% and 13% exhibited significant differences in H3K9me3 enrichment. These changes mapped onto gene networks regulating synaptic plasticity, neuroinflammation, and reward circuits. Motif analysis of differentially modified genomic sites revealed significantly stronger choline effects than early-life ID and identified multiple epigenetically modified transcription factor binding sites.

Conclusions This study reveals genome-wide, stable epigenetic changes and epigenetically modifiable gene networks associated with specific chromatin marks in the hippocampus, and lays a foundation to further elucidate iron-dependent epigenetic mechanisms that underlie the long-term effects of fetal-neonatal ID, choline, and their interactions.

Keywords Iron deficiency, Choline, Chromatin accessibility, H3K9me3 ChIP-seq, Hippocampus, Epigenetics, Transcription

*Correspondence:
Phu V. Tran
tranx271@umn.edu
Full list of author information is available at the end of the article

Liu *et al. BMC Genomics*   (2024) 25:301

Page 2 of 17

Background

Iron deficiency (ID) during the gestational and neonatal periods, during which the brain undergoes robust growth [1–3], results in both short- and long-term neurodevelopmental impairments. The acute effects are understandable given the role(s) of iron in neuronal energy metabolism, myelination and neurotransmitter synthesis. The presence of long-term effects in spite of iron treatment in the neonatal period remain unexplained and represent the true cost to society in terms of educational attainment and personal productivity. Extensive longitudinal studies of human cohorts have uncovered a pattern of persistent cognitive impairment and emotional dysregulation following early postnatal ID despite treatment with iron-replacement therapy in childhood [4, 5]. In addition, emerging evidence suggests a significant association between maternal ID and risk of neurodevelopmental disorders such as autism spectrum disorder, attention-deficit hyperactive disorders, and schizophrenia in the offspring [6–9]. Animal models of fetal-neonatal ID exhibit analogous neurodevelopmental impairments and show persistent and widespread gene dysregulation in the adult hippocampus [10–31]. The long-term gene expression changes suggest stable changes in the epigenome as a potential mechanism of action.

The persistence of negative gene expression changes and neurobehavioral phenotypes in preclinical models despite iron treatment commenced in the neonatal period confirms that iron treatment alone is insufficient to completely mitigate the early-life ID effects observed in the clinical populations. Thus, adjunctive therapy is needed for the treatment of early-life ID to rescue the poor long-term neurologic outcomes beyond the already too late iron replacement therapy. In this regard, choline supplementation has been shown to mitigate the deleterious developmental effects of early-life adverse exposures and aberrant genetic factors on brain development [32–35], including fetal alcohol syndrome where brain iron metabolism is perturbed [36, 37]. Choline is an essential nutrient for brain development and can act as a methyl donor to modify DNA and histone methylation [38–43]. In the context of fetal-neonatal ID, choline supplementation has been shown to partially rescue ID-induced abnormal cognitive function and hippocampal transcriptomic and epigenomic changes [12, 24, 25, 44]. The findings suggest an interaction between these two essential nutrients in regulating the brain epigenomic landscape. However, epigenome-wide changes in chromatin accessibility and histone modification due to early-life ID or its treatment with choline supplementation have not been interrogated.

In the present study, we employed Next-Generation Sequencing to assess fetal-neonatal ID-induced global changes in accessible chromatin [45] by Assay for Transposase Accessible Chromatin with sequencing (ATAC-seq). This approach is powered by its unbiased manner to assess chromatin accessibility changes for transcription factor (TF) binding sites. Besides, our previous study demonstrated that early-life ID and prenatal choline altered H3K9me3 enrichment (an index of epigenetic gene silencing [46]) at the iron-dependent histone modifier site [44]. Therefore, in this study we performed a comprehensive investigation of histone H3K9me3 signature at an epigenome-wide level by Chromatin Immunoprecipitation with sequencing (ChIP-seq) and assessed the effects of prenatal choline on these ID-induced epigenetic changes. We hypothesized that fetal-neonatal ID induces changes in chromatin accessibility and H3K9me3 landscapes, which would coincide with, and therefore likely contribute to, the lasting gene dysregulation. Time-targeted prenatal choline-supplementation would normalize multiple early-life ID-induced epigenetic changes. Based on the long-term clinical effects of ID, we predicted that these changes would occur in gene networks regulating neurocognition and emotional behaviors.

Results

Fetal-neonatal ID and prenatal choline supplementation alter long-term chromatin accessibility in the adult rat hippocampus

To elucidate the long-term changes in genome-wide chromatin accessibility due to fetal-neonatal ID or prenatal choline supplementation, P65 adult rat hippocampus was analyzed by ATAC-seq. Compared to the IS control group, the FID, FIDch or ISch groups showed significant differential sites assigned to known genes with more instances of increased than decreased accessibility (Fig. 1A). Prenatal choline resulted in a higher number of accessible loci in the FIDch compared to the untreated FID group (Fig. 1A, FIDch vs. FID). While these changes occurred across the whole genome, greater proportions occurred within the gene body and the intergenic regions (Fig. 1B).

To define the biological significance of the changes in chromatin accessibility, we employed IPA to functionally annotate the altered loci. Top hierarchically ranked annotated biofunctions showed that fetal-neonatal ID increased accessibility of genes regulating cell proliferation (Fig. 1C, FID/IS) but decreased accessibility of loci regulating neuronal maturation (Fig. 1C, FID/IS). These changes were mitigated by choline treatment (Fig. 1C, FIDch/IS). Choline also increased accessibility of loci implicated in myelination, release of vesicles, and transport of mitochondria and decreased accessibility of genes

Liu *et al. BMC Genomics*   (2024) 25:301

Page 3 of 17

regulating hippocampal cell death, synaptic long-term depression (LTD) of hippocampus, and gliosis of central nervous system (Fig. 1C, FIDch/IS). Choline treatment of the IS group decreased accessibility of genes regulating hippocampal formation, cell migration, synaptic structures and functions, and neuron proliferation and development (Fig. 1C, ISch/IS).

We next used IPA to annotate accessible loci altered by fetal-neonatal ID or choline treatment onto known canonical pathways. Fetal-neonatal ID results in increased chromatin accessibility of loci in energy metabolism, including fatty acid metabolism and mitochondrial function, but decreased accessibility of loci regulating synaptic signaling (synaptogenesis and LTD) and neurodevelopment (cAMP response element-binding protein [CREB] and prolactin signaling) (Fig. 1D, FID/IS). Choline treatment partially normalized these effects and increased accessibility of loci critical for neuroprotection (e.g., ephrin receptor and neurotrophin/tyrosine receptor kinase [TRK] signaling pathways) and neuroinflammation (interleukin [IL] -8 and transforming growth factor [TGF] -β signaling pathways) in the FIDch group (Fig. 1D, FIDch/IS). In the ISch group, choline treatment increased accessibility of loci in sphingosine-1-phosphate signaling and decreased accessibility of loci in the androgen, calcium and netrin signaling pathways (Fig. 1D, ISch/IS).

To identify gene targets that are epigenetically regulated by both iron and choline, we determined the common loci that were altered in adult FID rats by fetal-neonatal ID and choline. We compared the FID/IS to FIDch/IS ATAC-seq datasets and found that approximately 50% of the loci altered in the FID group were also altered in the FIDch group (Fig. 1E). These common loci mapped onto signaling pathways that regulate synaptic plasticity (mitogen-activated protein kinase [MAPK], calcium, synaptic LTD), energy metabolism (mammalian target of rapamycin [mTOR], transport of mitochondria),

neuroinflammation (IL-8, netrin signaling), and reward signaling (endocannabinoid, opioid) (Fig. 1E). Choline treatment not only rescued multiple fetal-neonatal ID effects but also increased (vs. always IS control) accessibility of loci regulating mitochondrial transport, IL-8 and mTOR signaling and decreased accessibility of loci that mapped onto pathways regulating synaptogenesis, hippocampal formation, neuron migration, and opioid signaling (Fig. 1E). 2336 loci showed choline-specific effects with increased accessibility of loci in signaling pathways regulating neuroinflammation (TGF-β, ciliary neurotrophic factor [CNTF], platelet-derived growth factor [PDGF], neuroglia development), synaptogenesis (RAC, ephrin receptor), and social behavior (oxytocin, endocannabinoid) and decreased accessibility of loci regulating astrocytosis and migration of cortical neurons (Fig. 1E).

Our previous transcriptomic study showed significant gene expression changes induced by prenatal choline in the IS adult rat hippocampus [12]. Consistent with these findings, the prenatal choline treated IS (ISch) group exhibited a substantial number of changes in loci accessibility that indicate decreased activity of a functional gene network associated with netrin signaling (Fig. 1F). These changes also showed an increase in sphingosine-1 phosphate signaling but decreases in the androgen and calcium signaling pathways (Fig. 1F, bottom table).

Prenatal choline increases enrichment of the repressive histone H3K9me3 across the adult rat hippocampal genome

To assess the long-term changes in repressive histone H3K9me3 signature due to either fetal-neonatal ID with or without prenatal choline, we performed an epigenome-wide ChIP-seq analysis of H3K9me3 in the adult P65 rat hippocampus. Compared to the IS control group, the FID group showed 1439 differential sites that were annotated to 199 genes, with 110 showing increased and 89 showing decreased H3K9me3

(See figure on next page.)

Fig. 1 Fetal-neonatal ID and prenatal choline supplementation altered chromatin accessibility landscape in P65 FID rat hippocampus. **A** ATAC-seq data showing differentially-accessible sites and associated genes between treatment groups. Numbers of differential sites include gene bodies, promoter regions (proximal, +1 K, +3 K), and intergenic regions. Selection criteria were absolute log2(Fold Change) > 0.2 and false discovery rate *q*-value < 0.05, *n* = 4/group. **B** Distribution of sites with differential accessibility. (C, D) Ingenuity Pathway Analysis (IPA) mapped loci with differential ATAC peaks (within gene bodies or promoter regions) onto biofunctions (**C**) and canonical signaling pathways (**D**), ranked hierarchically. Comparisons were made among formerly iron-deficient (FID), formerly iron-deficient with choline (FIDch), and iron-sufficient with choline (ISch) normalized by the iron-sufficient (IS) control group. Squares with dots have absolute z-scores < 2.0, indicating non-significant findings. Blue and orange colors indicate decreased and increased chromatin accessibilities, respectively. Fewer changes were found in the FID compared to FIDch and ISch groups (absolute z-scores > 2.0). Choline induced both decreased and increased chromatin accessibility in the FIDch and ISch groups. **E** Venn diagram showing overlap and non-overlapping genes modified in FID and FIDch groups. +/−/n indicates increased, decreased, and normalized changes in ATAC signatures. Blue and orange indicate decreased and increased ATAC signatures, respectively. **F** Comparison between ISch and IS control group showing the choline effect on ATAC landscape in adult rat hippocampus. IPA generates a graphical summary showing decreased accessibility in loci regulating hippocampal and cortical development centered on microtubule dynamics and canonical pathways showing both increased and decreased ATAC signatures

Fig. 1 (See legend on previous page.)

Liu *et al. BMC Genomics*   (2024) 25:301

Page 5 of 17
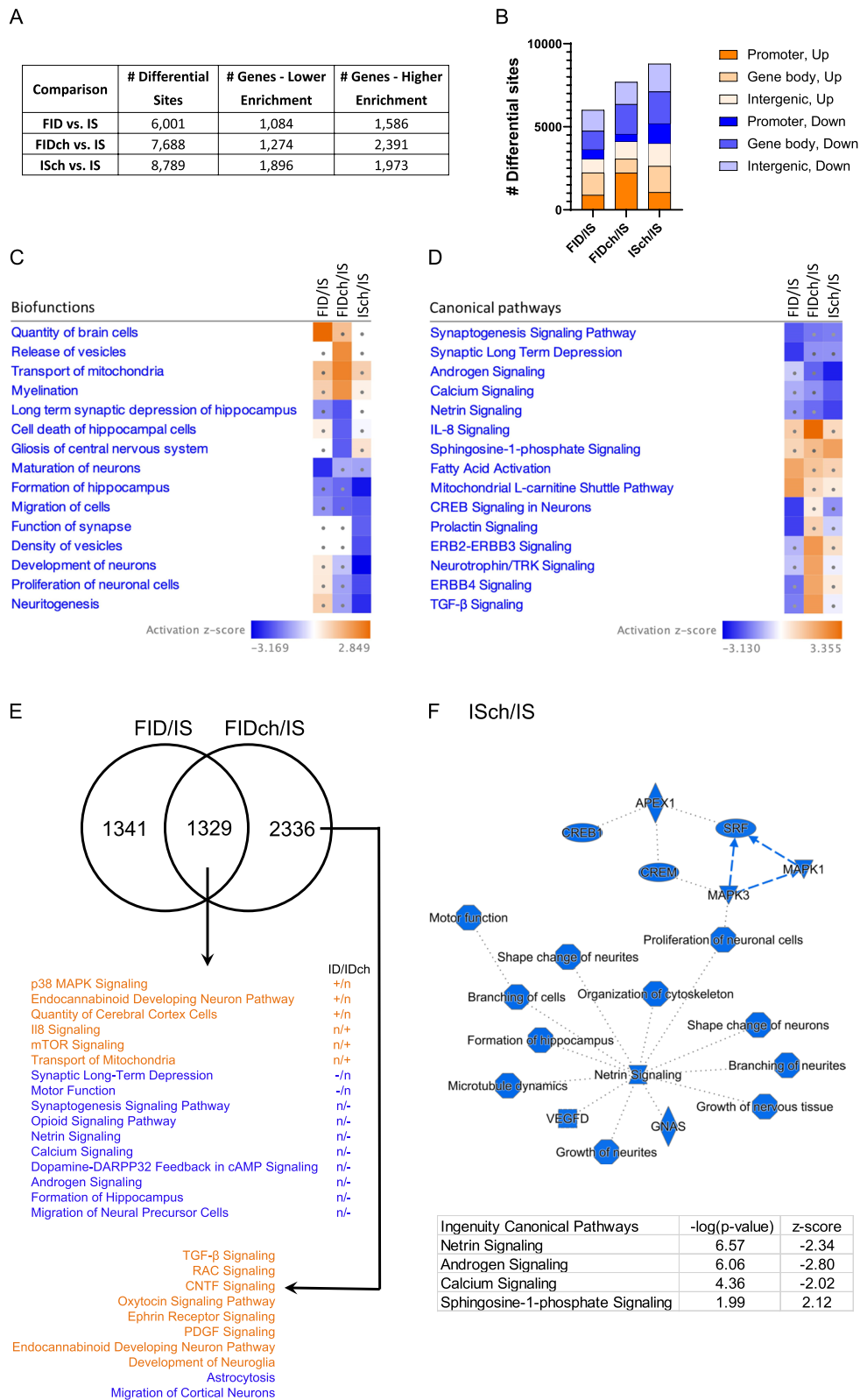
enrichment (Fig. 2A). Both FIDch and ISch groups showed ~ 23,000 differential sites that mapped onto 2451 and 3435 loci, respectively, based on changes at the promoters and within gene bodies (Fig. 2A). Changes in H3K9me3 enrichment occurred predominantly in the intergenic regions (Fig. 2B).

We then analyzed H3K9me3 changes that mapped onto known genes using IPA. While fetal-neonatal ID alone showed no significant changes of specific biofunctions in the FID group (Fig. 2C, FID/IS), choline treatment exhibited substantial H3K9me3 enrichment changes in the FIDch and ISch groups (Fig. 2C, FIDch/IS and ISch/IS). Enrichment changes in the FIDch group indicate major effects with an increase in loci regulating microtubule dynamics, neurodevelopment, neuritogenesis, neurotransmission, and apoptosis of neurons but a decrease in loci regulating neuronal viability (Fig. 2C, FIDch/IS). The ISch group exhibited even greater H3K9me3 enrichment changes than the FIDch group with an increase at additional loci regulating differentiation of neural cells including oligodendrocytes and synaptic plasticity (e.g., transport of synaptic vesicles, long-term potentiation [LTP], synaptic LTD, quantity of synapse), and a decrease in loci regulating behavioral deficit (Fig. 2C, ISch/IS).

Regarding the canonical signaling pathways, fetal-neonatal ID increased H3K9me3 enrichment at loci regulating coordinated lysosomal expression and regulation (CLEAR), neurovascular coupling, and autophagy pathways (Fig. 2D, FID/IS). Prenatal choline not only rescued the multiple fetal-neonatal ID effects but also increased H3K9me3 enrichment at loci regulating neuroendocrine signaling (corticotropin-releasing hormone, estrogen receptor), synaptic plasticity (synaptogenesis, ephrin receptor, SNARE) and neuroinflammation (IL-15 production) in the FIDch group (Fig. 2D, FIDch/IS). These enrichment changes were choline-specific as the ISch group also showed increased in many of the same pathways along with additional pathways, notably prolactin, oxytocin, nerve growth factor (NGF), and CREB signaling (Fig. 2D, ISch/IS).

To further identify loci and associated biofunctions in adult rats that were altered by both fetal-neonatal ID and choline, we analyzed the overlapping genes in the FID and FIDch datasets. 126 loci were identified and showed decreased enrichment in signaling associated with damaged tissue repair in the FIDch group compared to FID group (Fig. 2E). The non-overlapping 2325 loci in the FIDch group showed higher H3K9me3 enrichment among loci regulating learning and memory (cognition, LTP, neurotransmission), development of neurons (synaptogenesis, microtubule dynamics, apoptosis of neurons, ephrin and estrogen receptor signaling) and IL-15 production (Fig. 2E).
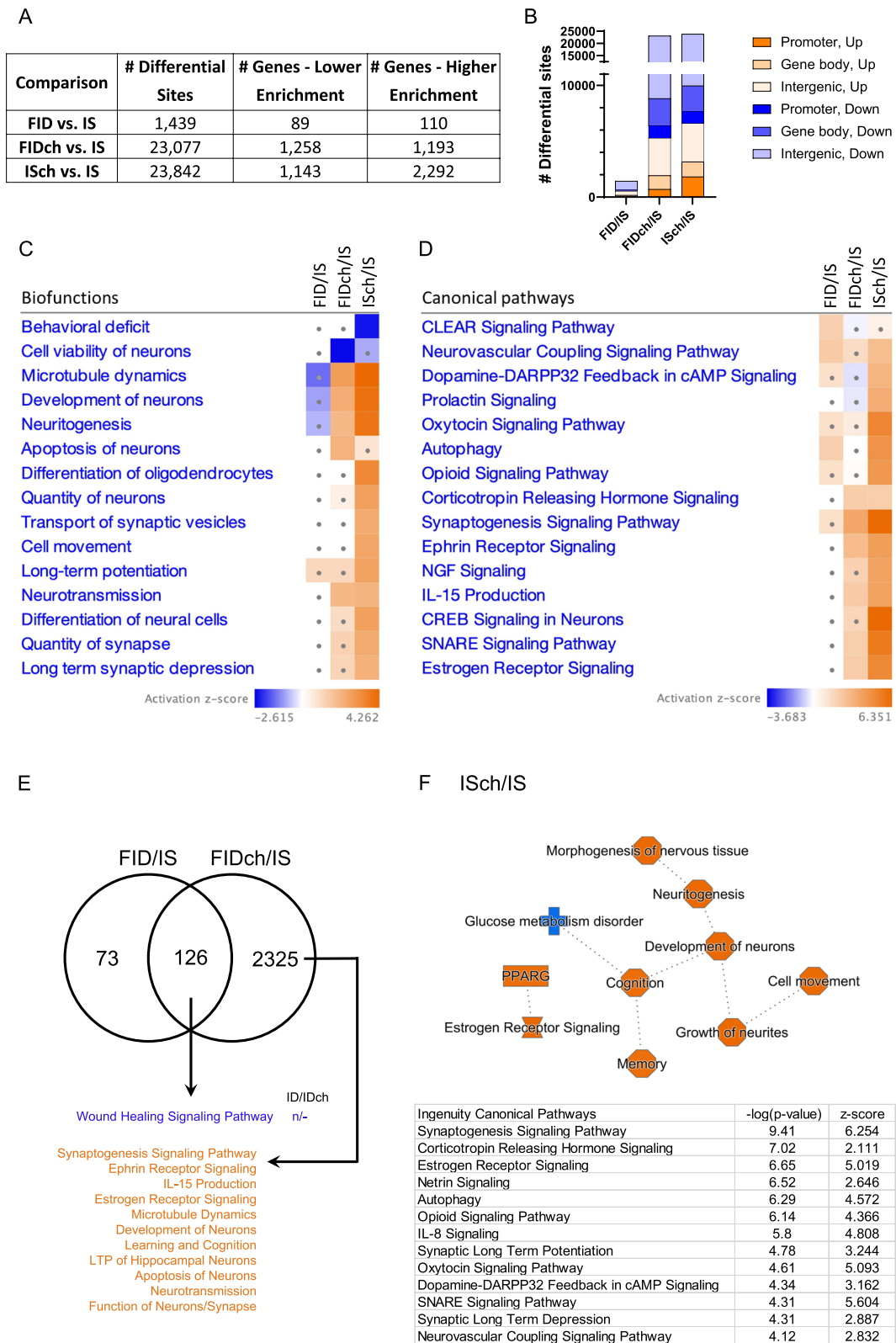
In the ISch group, H3K9me3 enrichment changes indicate overall increases among loci regulating neuronal development (neuritogenesis, cell movement), and social cognition (memory, oxytocin, estrogen, corticotrophin-releasing hormone [CRH]) as well as signaling pathways regulating synaptic transmission (synaptogenesis, synaptic LTD, LTP, SNARE, neurovascular coupling), reward processing (opioid, dopamine-DARPP32 feedback), and neuroinflammation (IL-8) (Fig. 2F).

Choline rescued fetal-neonatal ID-induced epigenomic changes through distinct regulatory mechanisms

ATAC- and ChIP-seq datasets were analyzed for chromatin accessibility and H3K9me3 enrichment at known TF binding motifs using HOMER motifs analysis in specific genomic regions (i.e., promoter, gene body, intergenic region), to investigate changes in these regulatory mechanisms induced by fetal-neonatal ID and choline supplementation. Compared to the IS group, both fetal-neonatal ID and choline treatment showed more motifs with increased (i.e., open chromatin and H3K9me3 mark) than decreased enrichment (Fig. 3A, B). Chromatin accessibility changes occurred predominantly

(See figure on next page.)

Fig. 2 Fetal-neonatal ID and prenatal choline supplementation altered histone H3K9me3 landscape in P65 FID rat hippocampus. **A** H3K9me3 ChIP-seq data showing differential sites and associated genes between treatment groups. Numbers of differential sites include gene bodies, promoter regions (proximal, +1 K, +3 K), and intergenic regions. Selection criteria were absolute log2(Fold Change) > 0.2 and false discovery rate q-value < 0.05, n = 4/group. **B** Distribution of sites with differential H3K9me3 enrichment. (C, D) Ingenuity Pathway Analysis (IPA) mapped differentially-enriched H3K9me3 loci onto biofunctions (**C**) and canonical signaling pathways (**D**), ranked hierarchically. Comparisons were made among formerly iron-deficient (FID), formerly iron-deficient with choline (FIDch), and iron-sufficient with choline (ISch) normalized by the iron-sufficient (IS) control group. Squares with dots have absolute z-scores < 2.0. Blue and orange colors indicate decreased and increased H3K9me3 enrichment, respectively. Early-life ID produced little changes in H3K9me3 signature (absolute z-scores < 2.0). Choline increased H3K9me3 enrichment in the FIDch and ISch groups. **E** Venn diagram showing overlap and non-overlapping genes modified in FID and FIDch groups. +/−/n indicate increased, decreased, and normalized changes in H3K9me3. Blue and orange indicate decreased and increased H3K9me3 signatures. **F** Comparison between ISch and IS control group showing the choline effect on H3K9me3 in adult rat hippocampus. IPA generates a graphical summary showing increased H3K9me3 in loci associated with cognition and estrogen receptor signaling, and canonical pathways showing significantly increased H3K9me3 enrichment

A

Comparison	# Differential Sites	# Genes - Lower Enrichment	# Genes - Higher Enrichment
FID vs. IS	1,439	89	110
FIDch vs. IS	23,077	1,258	1,193
ISch vs. IS	23,842	1,143	2,292

B

C

Biofunctions

Behavioral deficit
Cell viability of neurons
Microtubule dynamics
Development of neurons
Neuritogenesis
Apoptosis of neurons
Differentiation of oligodendrocytes
Quantity of neurons
Transport of synaptic vesicles
Cell movement
Long-term potentiation
Neurotransmission
Differentiation of neural cells
Quantity of synapse
Long term synaptic depression

D

Canonical pathways

CLEAR Signaling Pathway
Neurovascular Coupling Signaling Pathway
Dopamine-DARPP32 Feedback in cAMP Signaling
Prolactin Signaling
Oxytocin Signaling Pathway
Autophagy
Opioid Signaling Pathway
Corticotropin Releasing Hormone Signaling
Synaptogenesis Signaling Pathway
Ephrin Receptor Signaling
NGF Signaling
IL-15 Production
CREB Signaling in Neurons
SNARE Signaling Pathway
Estrogen Receptor Signaling

E

FID/IS   FIDch/IS

73   126   2325

ID/IDch
n/-

Wound Healing Signaling Pathway

Synaptogenesis Signaling Pathway
Ephrin Receptor Signaling
IL-15 Production
Estrogen Receptor Signaling
Microtubule Dynamics
Development of Neurons
Learning and Cognition
LTP of Hippocampal Neurons
Apoptosis of Neurons
Neurotransmission
Function of Neurons/Synapse

F   ISch/IS

Ingenuity Canonical Pathways	-log(p-value)	z-score
Synaptogenesis Signaling Pathway	9.41	6.254
Corticotropin Releasing Hormone Signaling	7.02	2.111
Estrogen Receptor Signaling	6.65	5.019
Netrin Signaling	6.52	2.646
Autophagy	6.29	4.572
Opioid Signaling Pathway	6.14	4.366
IL-8 Signaling	5.8	4.808
Synaptic Long Term Potentiation	4.78	3.244
Oxytocin Signaling Pathway	4.61	5.093
Dopamine-DARPP32 Feedback in cAMP Signaling	4.34	3.162
SNARE Signaling Pathway	4.31	5.604
Synaptic Long Term Depression	4.31	2.887
Neurovascular Coupling Signaling Pathway	4.12	2.832

Fig. 2 (See legend on previous page.)

Liu *et al. BMC Genomics*   (2024) 25:301

Page 7 of 17

in motifs located within the promoter and gene body regions, whereas H3K9me3 changes were primarily found in motifs within the intergenic regions (Fig. 3A, B). As expected, very few motifs were overlapped between ATAC- and ChIP-seq datasets, except for those associated with increased enrichment in the promoter region in ISch groups, indicating mutually exclusive actions of the two epigenetic marks (i.e., activation vs. suppression, Supplemental Fig. S1). Most fetal-neonatal ID-increased motif accessibility at promoter regions were not normalized by choline (FIDch, Fig. 3C); similarly, those changes were also induced by choline-supplemented IS rats (ISch, Fig. 3C). In contrast, choline supplementation normalized the fetal-neonatal ID-reduced H3K9me3 enrichment in motifs found within the intergenic regions (FIDch, Fig. 3D). Such effects were driven primarily by choline as shown by a major overlap of motifs between the choline-treated groups (ISch vs FIDch, Fig. 3D, Supplemental Fig. S2).

Since the functions of TF binding motifs were best characterized at the promoter region, we focused the functional analysis of these specific motifs. Common motifs among the 3 experimental groups showed increased accessibility (ATAC) for TFs involved in mitochondrial function (RONIN) and neurite outgrowth and neural development (SP1/KLF, E2F, CTCF, BORIS) (Fig. 3C, E; Supplemental Figs. S3-5). Choline-specific effect regardless of fetal-neonatal iron status includes increased accessibility of TFs involved in neurodegeneration (HINFP), oxidative phosphorylation (NRF1), and CNS development (ELF1, YY1, ELK) (Fig. 3F; Supplemental Fig. S4–5). The choline-supplemented FID group (FIDch) showed increased accessibility of TFs involved in neuroinflammation (IRF, NFIL3) and the development of GABAergic and dopaminergic neuron (FOXA1, DLX) (Fig. 3G, Supplemental Fig. S4). One member from the IRF family (IRF2) also showed increased accessibility in the ISch group (q-value = 0.0017, Supplemental Fig. S5).

Integration of RNA-seq, ATAC-seq, and ChIP-H3K9me3-seq data revealed an increase of synaptic transmission in adult rat hippocampus due to early-life ID or prenatal choline supplementation

Congruency of transcriptomic and epigenomic signatures was determined between each treatment (FID, FIDch or ISch) and control (IS) group to further elucidate altered biofunctions and canonical pathways. In the FID group, 159 (22%) loci showed changes in both expression and chromatin accessibility, indicating increased synaptic functions (synaptic transmission, synaptic depression, and LTP) and decreased neural cell migration, neurite branching, and emotional behaviors (Fig. 4A). In the FIDch group, 197 (24%) and 88 (13%) differentially expressed (DE) genes also showed change in chromatin accessibility and H3K9me3, respectively (Fig. 4B). These changes indicate an increased in neurodevelopment, cell movement, neuroglia quantity, and cellular functions (Fig. 4B). In the ISch group, 210 (29%) and 155 (24%) DE genes showed changes in chromatin accessibility and H3K9me3, respectively, that indicate reduced neural and axonal development and enhanced cell migration, synaptic transmission, and memory (Fig. 4C). The 107 common loci that were changed in both ATAC and H3K9me3 from the ISch group showed expression changes indicating increased cell quantity and synaptic transmission (Fig. 4C).
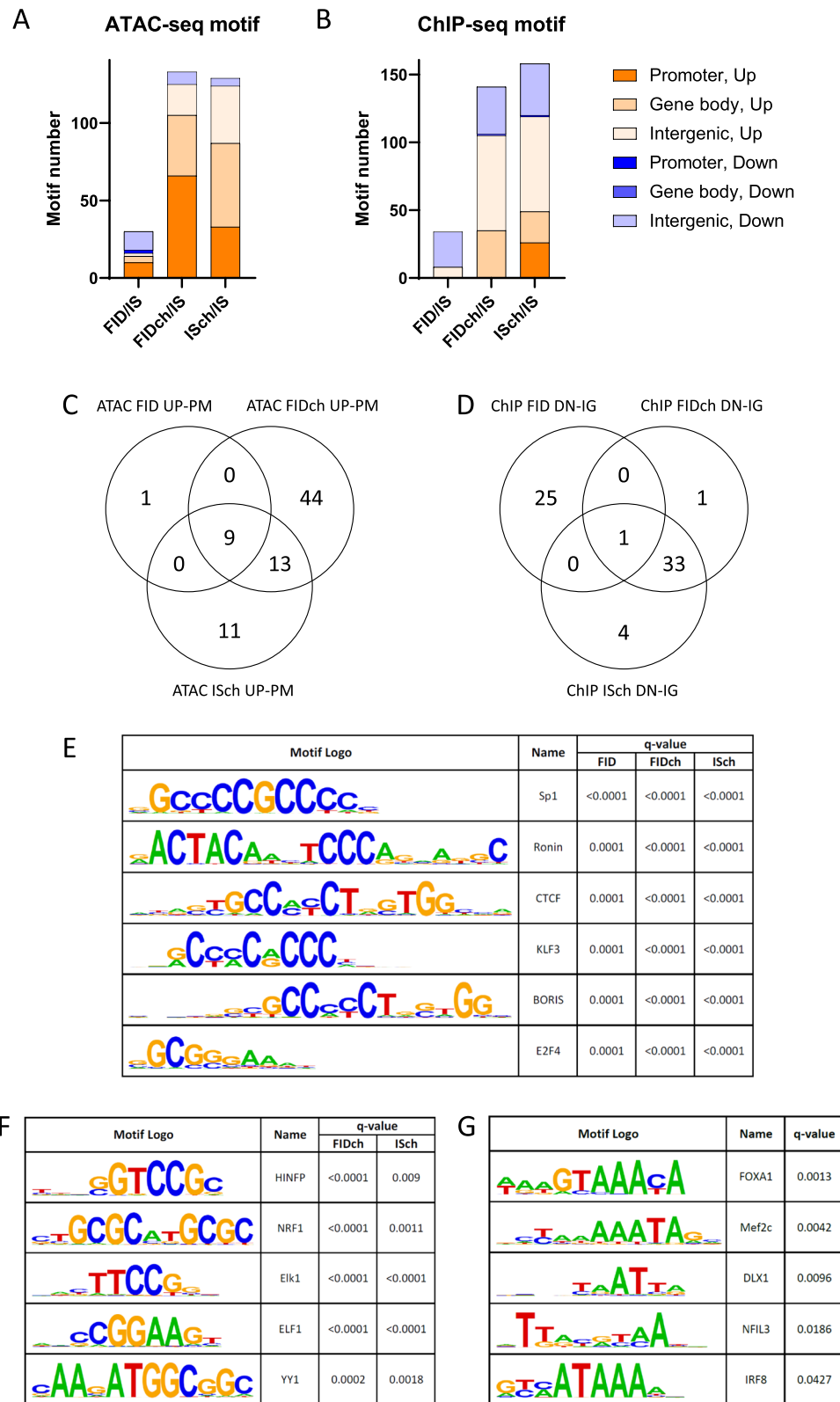
Since ATAC and H3K9me3 peaks showed overlap mainly in the intergenic regions across all four experimental groups (Table 1), we analyzed the nearest genes to these overlapping regions and identified 91 common genes among IS, FID and FIDch groups. These genes mapped onto a network centering on brain-derived neurotrophic factor (BDNF), presenilin-1 (PSEN1), and amyloid precursor protein (APP) (Fig. 5A). The choline-specific effect showed 142 genes that mapped onto a network centering on alpha-synuclein (SNCA), Huntingtin (HTT), transcription factor 7 like 2 (TCF7L2), and interferon gamma (INFG) (Fig. 5B).

Discussion

Early-life ID and prenatal choline produce persistent and widespread hippocampal gene dysregulation in preclinical models [11, 12, 47]. We previously demonstrated DNA methylation changes in the developing iron-deficient hippocampus [48] and chromatin methylation changes at the *Bdnf* gene in the FID hippocampus [12], providing evidence for acute and persistent epigenetic modifications induced by early-life ID. To systematically determine the stable long-term epigenetic changes induced by early-life ID in the iron-repleted adult hippocampus,

---

(See figure on next page.)

Fig. 3 Motif analysis of sites with fetal-neonatal ID-altered chromatin accessibility and H3K9me3 signatures. **A**, **B** Numbers and distributions of motifs identified in each dataset. **C** Overlap of motifs with increased (UP) accessibility in the promoter region (PM) among the 3 experimental groups. **D** Overlap of motifs with decreased (DN) enrichment of H3K9me3 mark the intergenic region (IG) among the 3 experimental groups. **E-G** Representative motifs with increased accessibility in the promoter region shared by FID, FIDch and ISch groups (**E**), only shared by FIDch and ISch groups (**F**), and exclusively in the FIDch group (**G**)

Liu *et al. BMC Genomics*   (2024) 25:301

Page 8 of 17

Fig. 3 (See legend on previous page.)

Liu *et al. BMC Genomics*   (2024) 25:301

Page 9 of 17

the present study assessed and integrated the landscapes of accessible chromatin modifications (ATAC vs. H3K9me3) and transcriptomic changes from the FID rat hippocampus. The findings reveal that fetal-neonatal ID altered chromatin accessibility accounting for about 22% of gene expression changes, particularly among loci that regulate neurite growth and synaptic transmission; however, fetal-neonatal ID had little (~1.7%) effect on the repressive histone H3K9me3 mark. These lower overlap percentages might partially be due to sampling from separate groups of animals, but could also indicate other mechanisms underlying the long-term gene expression changes, suggesting an involvement of other epigenetic modifications. Thus, integration of additional epigenetic marks (e.g., H3K27me3, H3K4me3, 5mC, and 5hmC [49, 50]) is needed in future studies to more fully elucidate epigenetic mechanisms contributing to the fetal-neonatal ID-induced long-term gene dysregulation.

We addressed the prenatal choline effects on specific epigenetic modifications given its initial identification as a potential adjunctive treatment for early-life ID [25, 51]. Choline partially rescued the fetal-neonatal ID effects, accounting for 24% of gene expression changes. Interestingly, prenatal choline had a significant effect on both ATAC and H3K9me3 changes in the IS group, particularly among loci regulating neurotransmission and opioid signaling, suggesting either excessive dosing or duration of choline treatment. Thus, more studies assessing choline dose-responses are needed in order to identify appropriate dosing for its proposed used as an adjunct therapy for early-life ID anemia [52]. Collectively, these findings reveal a lasting consequence of early-life ID and prenatal choline on the adult male rat hippocampal epigenome.

Fetal-neonatal ID resulted in more loci showing increased than decreased accessibility, consistent with our transcriptomic data. These findings support the conclusion that changes in ATAC partially account for the long-term epigenetic modifications induced by early-life ID [53]. Nevertheless, it is not surprising that the reduced chromatin accessibility occurred among loci regulating maturation of hippocampal neurons, which may account

for the impaired cognitive function exhibited by FID rats [24, 25]. Our group recently reported the effect of phlebotomy-induced ID anemia on neuroinflammation [54]. Given the important role of microglia in neural development and function [55], the long-term ID-induced epigenetic changes in loci regulating neuroinflammation signaling pathways could contribute to the abnormal cognition, emotional behavior, and neurodevelopmental disorders (e.g., autism, schizophrenia, Alzheimer disease) observed in the FID adult animals [21, 26, 29].

The established beneficial effects of prenatal choline demonstrated by others in preclinical models of other neurodevelopmental conditions [33–35, 41], by us in this model of fetal-neonatal ID [12, 51] and clinically in children [32], as well as choline's role as a methyl donor [56] justified the rationale for assessing its long-term effects on the neuroepigenome. A major finding was of long-term choline effects on both ATAC and H3K9me3 landscapes in the hippocampus of the FID and IS control groups. In the FID group, choline supplementation not only normalized fetal-neonatal ID-reduced accessibility of genes that regulate neuronal maturation and synaptic plasticity (e.g., synaptogenesis, LTD, CREB signaling pathways) but also promoted accessibility of genes regulating myelination, mitochondrial transport, and synaptic function (ephrin and neurotrophin signaling). These effects could account for the partial recovery of hippocampal-dependent learning and memory function in FIDch adult rats [51]. While these long-term epigenetic changes were found in the hippocampus, a focus of our study, they could also occur in the cerebral cortex and cerebellum as these brain structures have a long developmentally-sensitive window [57]. Future studies could investigate the epigenomic effects of early-life ID on other developing brain regions as we have in a previous study [58].

A novel and unique finding of prenatal choline effect in the IS group (ISch) was the increased H3K9me3 enrichment among loci regulating opioid and dopamine-DARPP32 signaling pathways, suggesting that choline can influence the reward circuitry potentially involving the hippocampal-cortical-nucleus accumbens

(See figure on next page.)

Fig. 4 Integration of P65 hippocampal RNA-seq, ATAC-seq, and ChIP-H3K9me3-seq data. **A** FID and IS comparison showing 159 of 731 (22%) loci with specific changes in chromatin accessibility. These changes indicate activated synaptic transmission and neuronal cell death accompanied by inhibited branching of neurites, migration of neural cells, and emotional behavior. **B** FIDch vs IS comparison showing 88 loci with specific H3K9me3 changes, which indicate an activated neuronal development. 197 loci with specific changes in chromatin accessibility indicate activated cellular function, including cellular homeostasis, cell movement, cell death, and quantity of neuroglia, but inhibited nerve degeneration. **C** ISch and IS comparison showing 107 loci with both ATAC and H3K9me3 changes, which indicate activated synaptic transmission and quantity of cells. 155 loci with specific H3K9me3 changes indicate reduced neuronal viability but activated development of neurons, neurotransmission, and cell migration. 210 loci with specific changes in chromatin accessibility indicate both inhibited degeneration and activated apoptosis of neurons via different set of genes, as well as activated development of the nervous system

Liu *et al. BMC Genomics*   (2024) 25:301

Page 10 of 17
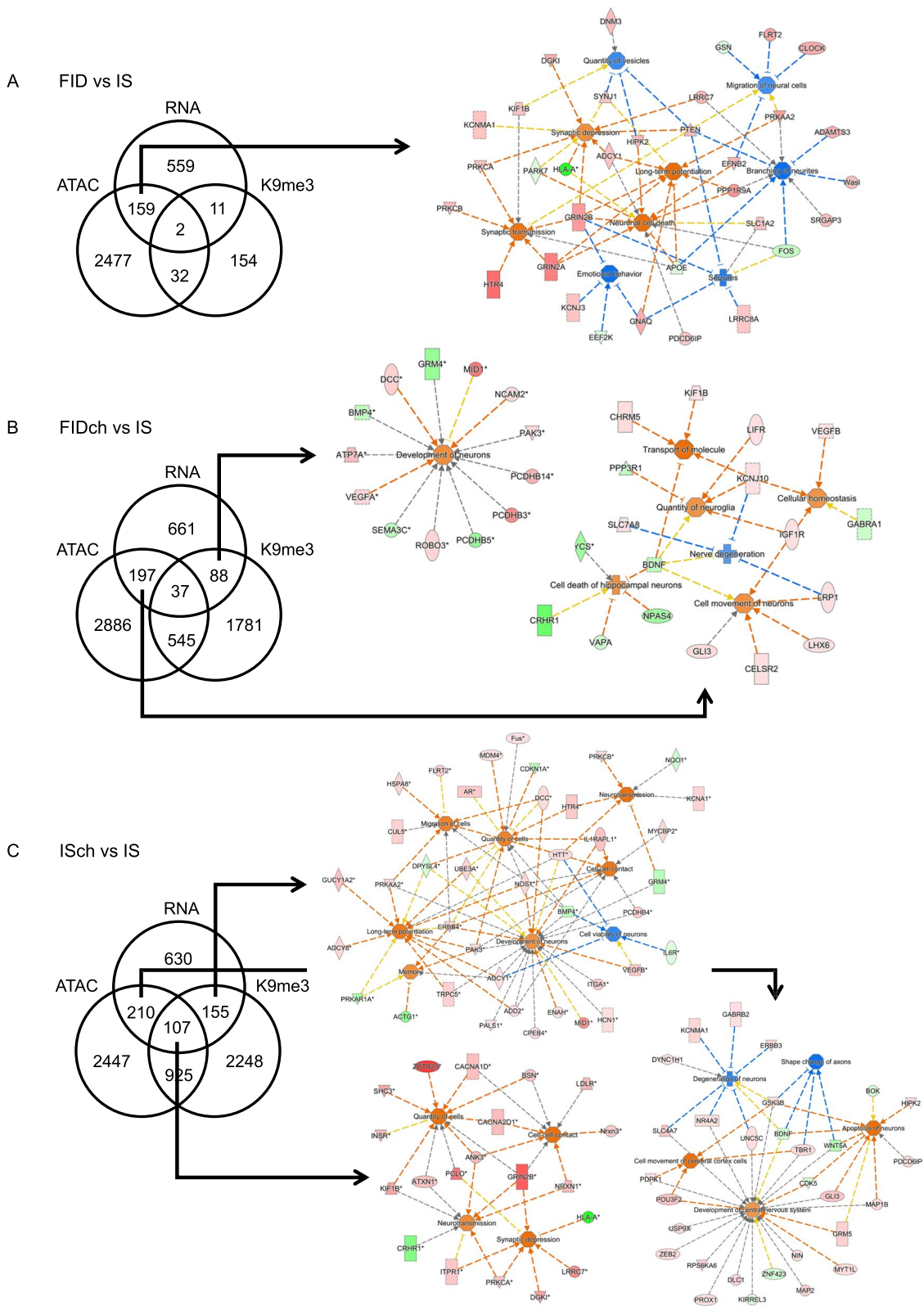
Fig. 4 (See legend on previous page.)

Table 1 Overlapping regions between ATAC and H3K9me3 peaks. The overlapping peaks between the two datasets were primarily located in intergenic regions

Treatment Group	# Overlapping Regions	# Nearest Loci	IPA-Annotated Diseases and Functions
IS	868	235	Development of CNS, Long-Term Potentiation (LTP)
ISch	593	237	Synaptic transmission of cerebrocortical cells, LTP of hippocampal neurons
FID	551	149	Differentiation of neurons, Migration of cells, LTP
FIDch	563	142	Cerebral disorder, Tauopathy, LTP, Migration of neuroglia
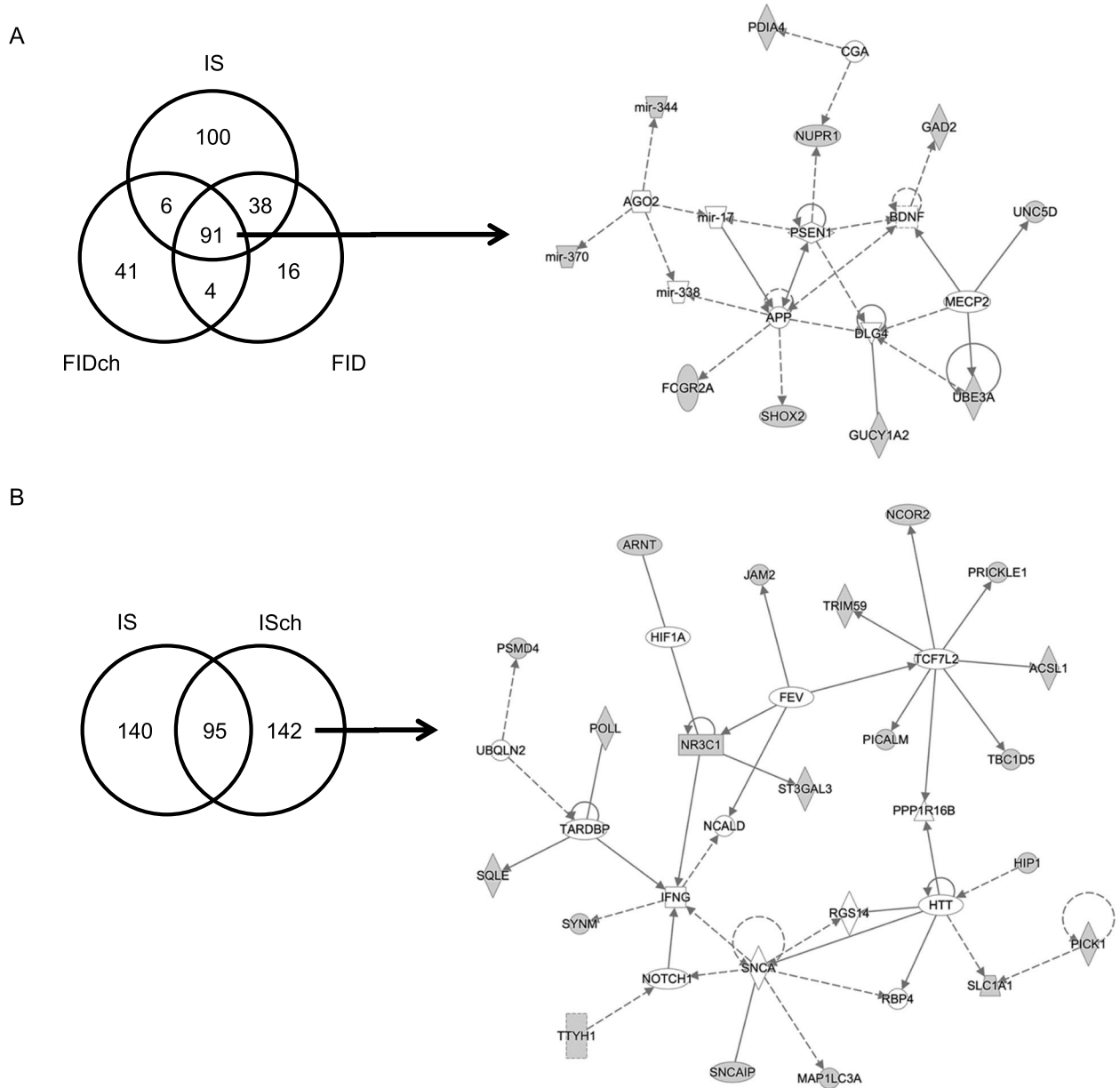
Fig. 5 Alignments of ATAC-seq and H3K9me3-seq peaks among treatment groups. **A** Overlapping ATAC and H3K9me3 peaks among IS, FID, and FIDch groups localized to the intergenic regions of 91 nearby genes, which mapped onto a gene network centering on the Brain-derived neurotrophic factor (BDNF), Presenilin-1 (PSEN1), and Amyloid precursor protein (APP), and methylcytosine-binding protein 2 (MeCP2). **B** Overlapping ATAC and H3K9me3 peaks between IS and ISch groups showed 142 choline-specific effect genes that mapped onto a gene network centering on alpha-synuclein (SNCA), Huntingtin (HTT), transcription factor 7 like 2 (TCF7L2), and interferon gamma (INFG)

Liu *et al. BMC Genomics*   (2024) 25:301

Page 12 of 17

connectivity [59, 60]. This finding raises possible concerns as to whether prenatal choline may affect the reward signaling circuity in adulthood given the chromatin changes in loci implicating altered balance of dopaminergic, glutamatergic, and GABAergic synaptic transmission [61–64]. Thus, the use of choline as a therapeutic agent will need more rigor scrutiny to determine the appropriate dose and duration during gestation so as to maximize the beneficial effects while minimizing potential negative impacts.

The fetal-neonatal ID or choline effects on ATAC and H3K9me3 signatures were largely distinct with limited overlapping regions, indicating that the majority of peaks between ATAC and H3K9me3 were mutually exclusive as expected given that they generally have opposing effects (activation vs. repression) on gene regulation [45, 46]. However, the genomic regions showing both ATAC and H3K9me3 changes by early-life ID were found in a gene network that include BDNF, APP, and PSEN1, which we have documented previously using transcriptomic and targeted gene expression analyses [21, 47]. The findings highlight convergent epigenetic modifications as well as reveal potential long-distance regulatory elements for specific gene networks that can be dysregulated by early-life ID. Likewise, prenatal choline produced convergent epigenetic modifications within a specific gene network regulating factors that contribute to neurological diseases, including SNCA, HTT, and NR3C1. Thus, it is important to determine the long-term neurological effects of prenatal choline supplementation to fully evaluate its beneficial effects beyond cognitive function. Lastly, analysis of fetal-neonatal ID and choline effects on TF binding motifs reveal that choline may rescue transcriptional and behavioral abnormalities induced by early-life ID using molecular machineries distinct from those directly affected by fetal-neonatal ID. TFs that were implicated only in the FIDch group such as FOXA1, DLX and certain members from the IRF family may serve as potential targets for the development of an interventional strategy to prevent long-term neurologic outcomes.

There are two limitations of our study. First, to keep in line with our prior behavioral analyses of this model, the study design involved culling litters and using a single male rat from each litter for the performed experiments. This was to minimize the effects associated with litter size and maternal nursing behavior. As such, this design potentially increases the variation of inherent epigenomes within the same experimental group, which could lead to smaller signal-to-noise ratio as epigenetic marks are shown to be heritable [65] and varied across litters. This inherent cross-litter variation in could pose a risk to the reproducibility of the study. Second, despite a statistical power of ∼70%, our experimental sample size ($n = 4$/

group), while similar to multiple published epigenetic studies [49, 66–70], could be underpowered to small differences between groups. Future studies could increase the sample size to 6/group, which would increase the estimated power to >80%, to detect these small changes.

Conclusions

Early-life ID produces lasting and widespread changes in the adult iron-repleted rat hippocampal epigenome, providing insights into molecular mechanisms mediating the long-term gene dysregulations. This study provides evidence that changes in chromatin accessibility could partially account for this persistent gene dysregulation in adulthood. The mechanisms underlying early-life ID-altered chromatin landscapes were likely independent of modifiers of H3K9me3 mark such as the iron-containing KDM4 histone demethylase and the G9A methyltransferase. Conversely, choline-mediated epigenetic changes in the rat hippocampus involved modification of the H3K9me3 landscape, implicating H3K9 methyltransferases and demethylases. Since epigenetic regulation involves complex interactions among iron-dependent and -independent factors, this study provides a foundation for further research to fully investigate the relative contributions of others epigenetic modifications underlying early-life ID-induced gene dysregulation and to identify potential therapeutic targets for the prevention of long-term adverse outcomes of early-life ID.

Methods

Animals

Gestational day (G) 2 pregnant Sprague-Dawley rats were purchased from Charles River Laboratories (Wilmington, MA). Rats were maintained on a 12-hr:12-hr light/dark cycle with ad lib food and water. Fetal-neonatal ID was induced by dietary manipulation as previously described [25, 71] to induce a degree of ID that occurs in human newborns [72]. In brief, pregnant rats were given a purified iron-deficient diet (4 mg Fe/kg, TD 80396, Harlan Teklad, Madison, WI) from G2 to postnatal day (P) 7 and a purified iron-sufficient diet (200 mg Fe/kg, TD 09256, Harlan Teklad) thereafter. Both diets were similar in all respects except for their ferric citrate content. Control iron-sufficient rats were generated from pregnant rats maintained on the iron-sufficient diet. Half of the dams on iron-sufficient or iron-deficient diet received dietary choline supplementation (5.0 g/kg choline chloride ([73, 74], Iron-sufficient + choline: TD 1448261, Iron-deficient + choline: TD 110139) from G11–18, while the remaining dams received iron-modified diets with standard choline content (1.1 g/kg). Thus, dams and their litters were randomly assigned to the following groups: iron-deficient with choline supplementation, iron-deficient without

Liu *et al. BMC Genomics*   (2024) 25:301

Page 13 of 17

choline supplementation, iron-sufficient with choline supplementation, and iron-sufficient without choline supplementation. All litters were culled to 8 pups at birth with equal numbers of male and female pups to minimize the effects associated with sex and litter size in maternal nursing behavior. Only male offspring were used in the current study. To avoid litter-specific effects, tissue from a single male rat from each litter was used in each experiment. Rats were weaned on P21 and maintained on an iron-sufficient diet thereafter. The pups were studied at P65 after complete brain iron repletion [75]. Therefore, the final study groups were formerly iron-deficient without choline supplementation (FID), formerly iron-deficient with choline supplementation (FIDch), iron-sufficient with choline supplementation (ISch), and always iron-sufficient without choline supplementation (IS, control group). The University of Minnesota Institutional Animal Care and Use Committee approved all experiments in this study (Protocol # 2001-37802A).

Hippocampal dissection

P65 rats were euthanized by injection of pentobarbital (100 mg/kg, intraperitoneal) followed by decapitation. Brains were removed and bisected along the midline on an ice-cold metal block. The hippocampus was isolated, flash-frozen in liquid nitrogen, and stored at $-80\,°C$.

Nuclei isolation and DNA transposition

Nuclei isolation and DNA transposition were carried out as previously described [76] with modifications. Briefly, flash-frozen hippocampus was thawed in cold homogenization buffer (5 mM $CaCl_2$, 3 mM $Mg(AC)_2$, 10 mM Tris pH 7.8, 0.0167 mM PMSF, 0.167 mM β-mercaptoethanol, 1x proteinase inhibitor (cOmplete), 320 mM sucrose, 0.1 mM EDTA, 0.1% CA630), and homogenized using a Pellet Pestle motor and syringe. Equal volume of 50% iodixanol solution (5 mM $CaCl_2$, 3 mM $Mg(AC)_2$, 10 mM Tris pH 7.8, 0.017 mM PMSF, 0.17 mM β-mercaptoethanol, 1x proteinase inhibitor (cOmplete), 50% iodixanol) was added to homogenate to reach a final concentration of 25% iodixanol. 29% (5 mM $CaCl_2$, 3 mM $Mg(AC)_2$, 10 mM Tris pH 7.8, 0.017 mM PMSF, 0.17 mM β-mercaptoethanol, 1x proteinase inhibitor (cOmplete), 160 mM sucrose, 29% iodixanol) and 35% (5 mM $CaCl_2$, 3 mM $Mg(AC)_2$, 10 mM Tris pH 7.8, 0.017 mM PMSF, 0.17 mM β-mercaptoethanol, 1x proteinase inhibitor (cOmplete), 160 mM sucrose, 35% iodixanol) iodixanol solution were sequentially added under the 25% iodixanol solution layer. The 3-layer system was centrifuged in a swinging bucket centrifuge at 4255 x g for 20 min. After centrifugation, nuclei were isolated and collected from the 29–35% iodixanol solution interface.

Isolated nuclei were counted with trypan blue (0.4%) and 50,000 nuclei were transferred into a tube containing 1 ml ATAC-RSB (10 mM Tris pH 7.8, 10 mM NaCl, 3 mM $MgCl_2$) with 0.1% Tween-20. Nuclei were pelleted by centrifugation at 500 x g for 10 min. All steps above were conducted on ice or at 4 °C. Nuclei were resuspended in transposition mix (25 μL 2x TD buffer (Illumina), 16.5 μL PBS, 0.5 μL 10% Tween-20, 1% digitonin, 2.5 μL Tn5 transposase (Illumina), 5 μL H_2O), and incubated at 37 °O for 30 min in a thermomixer at 1000 rpm. Transposed DNA was purified using MinElute Reaction Cleanup kit (Qiagen).

Chromatin immunoprecipitation (ChIP)

ChIP experiments were performed as previously described [77] with modifications. In brief, chromatin was prepared from hippocampal samples following the manufacturer's recommendations (Millipore, Temecula, CA). Samples were homogenized in ice-cold PBS (500 μL) using a Pellet Pestle motor and pelleted by centrifugation at 13 K rpm (30s). The pellets were resuspended in PBS and cross-linked in 1% formaldehyde solution (Sigma). Following the removal of fixative and PBS rinses, lysates were resuspended in 500 μL lysis buffer (1% SDS, 10 mM EDTA, 50 mM Tris pH 8.1, 1 mM PMSF, 10 μL 10X protease inhibitor cocktails (Roche, Indianapolis, IN)), incubated in an ice bath for 10 min, and sonicated (Bioruptor Pico, Diagenode) to shear DNA. Sonicated lysates were diluted 10-fold with ChIP dilution buffer (0.01% SDS, 1.1% Triton X-100, 1.2 mM EDTA, 16.7 mM Tris-pH 8.1, 167 mM NaCl) and pre-cleared with 75 μL of Protein A agarose (50% slurry, Sigma). Pre-cleared chromatin lysate was immunoprecipitated by a ChIP-grade rabbit polyclonal antibody against histone H3K9me3 (Cat. # C15410193, Diagenode) with end-over-end rotation (4 °C, overnight). The antibody-histone complex was collected through the addition of 75 μL Protein A agarose slurry with mixing (4 °C, ≥ 1 hour). Following washes (per manufacturer's protocol, Millipore), the immune-histone complex was eluted in 500 μL of elution buffer (1% SDS, 0.1 M $NaHCO_3$). Reverse cross-linking was achieved by incubation in NaCl (0.2 M, 65 °C, overnight). Protease digestion (20 μg proteinase K, 20 mM EDTA, 100 mM Tris-pH 6.5, 45 °C, 1 hour) was performed to recover DNA, which was further purified using phenol/chloroform extraction and EtOH precipitation (1/10 volume 3 M sodium acetate, pH 5.2, 2 volume ethanol). Levels of enriched *Gapdh* (active) and *Myod1* (inactive) loci were used to validate ChIP experiments by real-time PCR.

Liu *et al. BMC Genomics*   (2024) 25:301

Page 14 of 17

Real-time PCR

For validation analysis of precipitated DNA from ChIP experiments, SYBR-green PCR (Fast SYBR green master mix, ABI) was used to amplify *Gapdh and Myod1*. Input DNA (10%) was used as a normalizer to account for input amount (ΔCt). Real-time PCR was performed with QuantStudio™ 5 (Thermo Fisher).

Next-generation sequencing

Recovered DNA from ATAC or ChIP was delivered to the University of Minnesota Genomics Center for quality control, library preparation and sequencing. DNA was first quantified using the PicoGreen dsDNA Assay Kit (Invitrogen). ATAC-seq library preparation was performed in accordance with the ATAC-seq protocol as described by Buenrostro et al. [78]. Library preparation for ChIP-seq was completed using ThruPLEX® DNA-Seq (Rubicon Genomics) kit. Libraries were assessed for quality using electrophoresis on an Agilent Bioanalyzer (Agilent) and size-selected for 200 ~ 800 bp fragments. Selected libraries were quantified again, and sequencing was performed at a depth of ~ 46 million reads per sample using NovaSeq 6000 for ATAC-seq, and a depth of ~ 25 million reads per sample using HiSeq 2500 for ChIP-seq to generate 50-bp pair-end reads.

Bioinformatics

ChIP-seq and ATAC-seq datasets, comprising 16 samples with 4 biological replicates in each condition (IS, ISch, FID, and FIDch) were aligned to the Ensembl v90 rat reference genome (rn6) using HISAT2 (v2.2.1) [79]. MACS (v2.1.0) was utilized to assess sites of chromatin accessibility in ATAC-seq samples and sites of H3K9me3 histone modification (peaks) for each of the 4 conditions [80]. MACS2 was run with parameters --bw 300 -p 1e-05 for the ChIP-seq data and -p 1e-05 --nomodel --shift 100 --extsize 200 for ATAC-seq data. diffReps [81] was utilized to find differential sites for the comparisons to the IS control group (FID, FIDch, or ISch vs. IS). diffReps was run with default parameters. Global analysis of overlapping between ATAC and H3K9me3 peaks was performed using BEDTools (PMID: 20110278) [82] with 1 bp overlapping threshold to identify regions modified by both markers. Differential sites were mapped to genes using the tool HOMER (PMID: 20513432) [83]. Visualization of alignments of ATAC and H3K9me3 peaks for representative genes *Bmp3*, *Tnks*, and *Ireb2* was performed using Integrative Genomics Viewer (Supplemental Fig. S6).

For RNA-seq data, datasets from a previous study [12] were reprocessed using FastQC and HISAT2 (v2.1.0). Gene quantification was done via featureCounts (PMID: 24227677) [84] to obtain the raw counts of reads mapping to genes. Differentially expressed genes (absolute log2(Fold Change) > 0.2 and *p*-value < 0.05) were identified using the edgeR (PMID: 19910308) [85] package in CLC Genomics Workbench software (Qiagen, Redwood City, CA) with a negative binomial generalized log-linear model fit to the raw read counts. Each experimental group (FID, FIDch or ISch) was compared to the IS control group. Parameter fitting was performed separately for each pairwise comparison. RNA-seq results were previously validated using real time PCR [12].

Ingenuity pathway analysis (IPA)

Differentially modified genes from pairwise comparisons between treatment and IS control group (e.g., FID vs. IS, FIDch vs. IS, and ISch vs. IS) were analyzed by IPA (Qiagen), a knowledge-based database of > 8 million findings, to identify pertinent pathways, gene networks, and biofunctions. Data were analyzed using core analysis with Fisher's exact test *p*-value $\leq$ 0.05 and absolute Z-score $\geq$ 2.0. Positive and negative Z-scores indicate increased and decreased activity, respectively.

HOMER motif analysis

The program 'findMotifsGenome.pl' from the tool HOMER (PMID: 20513432) [83] was utilized to identify motifs of transcription factors among differential sites identified by diffReps (PMID: 23762400) [81] after applying an absolute log2(Fold Change) cutoff of 0.2 and an adjusted *p*-value cutoff of 0.05 [83].

Abbreviations

APP	Amyloid precursor protein
ATAC	Assay for transposase-accessible chromatin
BDNF	Brain-derived neurotrophic factor
ChIP	Chromatin immunoprecipitation
CLEAR	Coordinated lysosomal expression and regulation
CNTF	Ciliary neurotrophic factor
CREB	cAMP response element-binding protein
CRH	Corticotrophin-releasing hormone
DE	Differentially expressed
FID	Formerly iron-deficient
FIDch	Formerly iron-deficient with choline
G	Gestational day
ID	Iron deficiency
IL	Interleukin
IPA	Ingenuity pathway analysis
IS	Iron-sufficient
ISch	Iron-sufficient with choline
LTD	Long-term depression
LTP	Long-term potentiation
MAPK	Mitogen-activated protein kinase
mTOR	Mammalian target of rapamycin
NGF	Nerve growth factor
P	Postnatal day
PDGF	Platelet-derived growth factor
PSEN	Presenilin
TF	Transcription factor

Liu *et al. BMC Genomics*   (2024) 25:301

Page 15 of 17

TGF   Transforming growth factor
TRK   Tyrosine receptor kinase

Supplementary Information

The online version contains supplementary material available at https://doi.org/10.1186/s12864-024-10230-4.

Supplementary Material 1.

Supplementary Material 2.

Supplementary Material 3.

Supplementary Material 4.

Supplementary Material 5.

Supplementary Material 6.

Availability of data and materials
The datasets generated and/or analysed during the current study are available in the Gene Expression Omnibus repository, GSE229266, GSE244208 (reviewer access token: mrepmwoebrwttsl).

Declarations

Ethics approval and consent to participate
The University of Minnesota Institutional Animal Care and Use Committee approved all experiments in this study (Protocol # 2001-37802A). All methods are reported in accordance with Animal Research: Reporting of In Vivo Experiments guidelines for the reporting of animal experiments.

Consent for publication
Not applicable.

Competing interests
The authors declare no competing interests.

Author details
[1]Department of Pediatrics, University of Minnesota, Minneapolis, MN 55455, USA. [2]Department of Psychology, University of Minnesota, Minneapolis, MN 55455, USA. [3]Icahn School of Medicine at Mount Sinai, New York, NY 10029, USA.

References
1. Kuzawa CW. Adipose tissue in human infancy and childhood: an evolutionary perspective. Yearb Phys Anthropol. 1998;41:177–209.
2. Li Z, Okamoto KI, Hayashi Y, Sheng M. The importance of dendritic mitochondria in the morphogenesis and plasticity of spines and synapses. Cell. 2004;119:873–87.
3. Fukumitsu K, Hatsukano T, Yoshimura A, Heuser J, Fujishima K, Kengaku M. Mitochondrial fission protein Drp1 regulates mitochondrial transport and dendritic arborization in cerebellar Purkinje cells. Mol Cell Neurosci. 2016;71:56–65.
4. Lozoff B, Smith JB, Kaciroti N, Clark KM, Guevara S, Jimenez E. Functional significance of early-life iron deficiency: outcomes at 25 years. J Pediatr. 2013;163:1260–6.
5. Lozoff B, Jimenez E, Hagen J, Mollen E, Wolf AW. Poorer behavioral and developmental outcome more than 10 years after treatment for iron deficiency in infancy. Pediatrics. 2000;105:e51.
6. Insel BJ, Schaefer CA, McKeague IW, Susser ES, Brown AS. Maternal iron deficiency and the risk of schizophrenia in offspring. Arch Gen Psychiatry. 2008;65:1136–44.
7. Schmidt RJ, Tancredi DJ, Krakowiak P, Hansen RL, Ozonoff S. Maternal intake of supplemental iron and risk of autism spectrum disorder. Am J Epidemiol. 2014;180:890–900.
8. Sørensen HJ, Nielsen PR, Pedersen CB, Mortensen PB. Association between Prepartum maternal Iron deficiency and offspring risk of schizophrenia: population-based cohort study with linkage of Danish National Registers. Schizophr Bull. 2011;37:982.
9. Wiegersma AM, Dalman C, Lee BK, Karlsson H, Gardner RM. Association of Prenatal Maternal Anemia with Neurodevelopmental Disorders. JAMA Psychiatry. 2019;76:1294.
10. Fretham SJB, Carlson ES, Georgieff MK. The role of iron in learning and memory. Adv Nutr. 2011;2:112–21.
11. Schachtschneider KM, Liu Y, Rund LA, Madsen O, Johnson RW, Groenen MAM, et al. Impact of neonatal iron deficiency on hippocampal DNA methylation and gene transcription in a porcine biomedical model of cognitive development. BMC Genomics. 2016;17:1–14.
12. Tran PV, Kennedy BC, Pisansky MT, Won KJ, Gewirtz JC, Simmons RA, et al. Prenatal choline supplementation diminishes early-life iron deficiency-induced reprogramming of molecular networks associated with behavioral abnormalities in the adult rat hippocampus. J Nutr. 2016;146:484–93.
13. Barks A, Hall AM, Tran PV, Georgieff MK. Iron as a model nutrient for understanding the nutritional origins of neuropsychiatric disease. Pediatr Res. 2019;85:176–82.
14. Barks A, Fretham SJB, Georgieff MK, Tran PV. Early-life neuronal-specific Iron deficiency alters the adult mouse hippocampal transcriptome. J Nutr. 2018;148:1521–8.
15. Bastian TW, von Hohenberg WC, Mickelson DJ, Lanier LM, Georgieff MK. Iron deficiency impairs developing hippocampal neuron gene expression, energy metabolism, and dendrite complexity. Dev Neurosci. 2016;38:264–76.
16. Beard J, Erikson KM, Jones BC. Neonatal iron deficiency results in irreversible changes in dopamine function in rats. J Nutr. 2003;133:1174–9.
17. Beard JL, Wiesinger JA, Connor JR. Pre- and postweaning iron deficiency alters myelination in Sprague-Dawley rats. Dev Neurosci. 2003;25:308–15.
18. Boksa P, Zhang Y, Nouel D, Wong A, Wong TP. Early development of Parvalbumin-, somatostatin-, and cholecystokinin-expressing neurons in rat brain following prenatal immune activation and maternal Iron deficiency. Dev Neurosci. 2016;38:342–53.
19. Bourque SL, Iqbal U, Reynolds JN, Adams MA, Nakatsu K. Perinatal iron deficiency affects locomotor behavior and water maze performance in adult male and female rats. J Nutr. 2008;138:931–7.
20. Brunette KE, Tran PV, Wobken JD, Carlson ES, Georgieff MK. Gestational and neonatal Iron deficiency alters apical dendrite structure of CA1 pyramidal neurons in adult rat Hippocampus. Dev Neurosci. 2010;32:238–48.
21. Carlson ES, Stead JDH, Neal CR, Petryk A, Georgieff MK. Perinatal iron deficiency results in altered developmental expression of genes mediating energy metabolism and neuronal morphogenesis in hippocampus. Hippocampus. 2007;17:679–91.
22. Felt BT, Beard JL, Schallert T, Shao J, Aldridge JW, Connor JR, et al. Persistent neurochemical and behavioral abnormalities in adulthood despite early iron supplementation for perinatal iron deficiency anemia in rats. Behav Brain Res. 2006;171:261–70.
23. Harvey L, Boksa P. Additive effects of maternal iron deficiency and prenatal immune activation on adult behaviors in rat offspring. Brain Behav Immun. 2014;40:27–37.
24. Kennedy BC, Dimova JG, Siddappa AJM, Tran PV, Gewirtz JC, Georgieff MK. Prenatal choline supplementation ameliorates the long-term

neurobehavioral effects of fetal-neonatal iron deficiency in rats. J Nutr. 2014;144:1858–65.

25. Kennedy BC, Tran PV, Kohli M, Maertens JJ, Gewirtz JC, Georgieff MK. Beneficial effects of postnatal choline supplementation on long-term neurocognitive deficit resulting from fetal-neonatal iron deficiency. Behav Brain Res. 2018;336:40–3.

26. Matveeva TM, Singh G, Gisslen TA, Gewirtz JC, Georgieff MK. Sex differences in adult social, cognitive, and affective behavioral deficits following neonatal phlebotomy-induced anemia in mice. Brain Behav. 2021;11.

27. McEchron MD, Cheng AY, Liu H, Connor JR, Gilmartin MR. Perinatal nutritional iron deficiency permanently impairs hippocampus-dependent trace fear conditioning in rats. Nutr Neurosci. 2005;8:195–206.

28. Nishikura N, Hino K, Kimura T, Uchimura Y, Hino S, Nakao M, et al. Post-weaning Iron deficiency in male rats leads to long-term hyperactivity and decreased Reelin gene expression in the nucleus Accumbens. J Nutr. 2020;150:212–21.

29. Pisansky MT, Wickham RJ, Su J, Fretham S, Yuan LL, Sun M, et al. Iron deficiency with or without anemia impairs prepulse inhibition of the startle reflex. Hippocampus. 2013;23:952–62.

30. Rudy MJ, Salois G, Cubello J, Newell R, Mayer-Proschel M. Gestational iron deficiency affects the ratio between interneuron subtypes in the postnatal cerebral cortex in mice. Development. 2023;150.

31. Schmidt AT, Waldow KJ, Grove WM, Salinas JA, Georgieff MK. Dissociating the long-term effects of fetal/neonatal Iron deficiency on three types of learning in the rat. Behav Neurosci. 2007;121:475–82.

32. Wozniak JR, Fuglestad AJ, Eckerle JK, Kroupina MG, Miller NC, Boys CJ, et al. Choline supplementation in children with fetal alcohol Spectrum disorders (FASD) has high feasibility and tolerability. Nutr Res. 2013;33:897–904.

33. Mellott TJ, Huleatt OM, Shade BN, Pender SM, Liu YB, Slack BE, et al. Perinatal choline supplementation reduces amyloidosis and increases choline acetyltransferase expression in the Hippocampus of the APP-swePS1dE9 Alzheimer's disease model mice. PLoS One. 2017;12.

34. Chin EWM, Lim WM, Ma D, Rosales FJ, Goh ELK. Choline rescues Behavioural deficits in a mouse model of Rett syndrome by modulating neuronal plasticity. Mol Neurobiol. 2019;56:3882–96.

35. Agam G, Taylor Z, Vainer E, Golan HM. The influence of choline treatment on behavioral and neurochemical autistic-like phenotype in Mthfr-deficient mice. Transl Psychiatry. 2020;10:1–14.

36. Smith SM, Virdee MS, Eckerle JK, Sandness KE, Georgieff MK, Boys CJ, et al. Polymorphisms in SLC44A1 are associated with cognitive improvement in children diagnosed with fetal alcohol spectrum disorder: an exploratory study of oral choline supplementation. Am J Clin Nutr. 2021;114:617–27.

37. Miller MW, Roskams AJI, Connor JR. Iron regulation in the developing rat brain: effect of in utero ethanol exposure. J Neurochem. 1995;65:373–80.

38. Davison JM, Mellott TJ, Kovacheva VP, Blusztajn JK. Gestational choline supply regulates methylation of histone H3, expression of histone methyltransferases G9a (Kmt1c) and Suv39h1 (Kmt1a), and DNA methylation of their genes in rat fetal liver and brain. J Biol Chem. 2009;284:1982–9.

39. Krzysztof Blusztajn J, J. Mellott T. Choline nutrition programs brain development via DNA and histone methylation. Cent Nerv Syst agents. Med Chem. 2012;12:82–94.

40. Fisher MC, Zeisel SH, Mar MH, Sadler TW. Perturbations in choline metabolism cause neural tube defects in mouse embryos in vitro. FASEB J. 2002;16:619–21.

41. Zeisel SH. Nutritional importance of choline for brain development. J Am Coll Nutr. 2004;23:621S-626S.

42. Cooney CA, Dave AA, Wolff GL. Maternal methyl supplements in mice affect epigenetic variation and DNA methylation of offspring. J Nutr. 2002;132(8 SUPPL):2393S-2400S.

43. Jirtle RL. The Agouti mouse: a biosensor for environmental epigenomics studies investigating the developmental origins of health and disease. Epigenomics. 2014;6:447–50.

44. Liu SX, Barks AK, Lunos S, Gewirtz JC, Georgieff MK, Tran PV. Prenatal Iron deficiency and choline supplementation interact to epigenetically regulate Jarid1b and Bdnf in the rat Hippocampus into adulthood. Nutrients. 2021;13.

45. Klemm SL, Shipony Z, Greenleaf WJ. Chromatin accessibility and the regulatory epigenome. Nat Rev Genet. 2019;20:207–20.

46. Ninova M, Tóth KF, Aravin AA. The control of gene expression and cell identity by H3K9 trimethylation. Development. 2019;146.

47. Tran PV, Fretham SJB, Carlson ES, Georgieff MK. Long-term reduction of hippocampal brain-derived neurotrophic factor activity after fetal-neonatal iron deficiency in adult rats. Pediatr Res. 2009;65:493–8.

48. Lien YC, Condon DE, Georgieff MK, Simmons RA, Tran PV. Dysregulation of neuronal genes by fetal-neonatal iron deficiency anemia is associated with altered DNA methylation in the rat hippocampus. Nutrients. 2019;11:1191.

49. Feng J, Shao N, Szulwach KE, Vialou V, Huynh J, Zhong C, et al. Role of Tet1 and 5-hydroxymethylcytosine in cocaine action. Nat Neurosci. 2015;18:536–44.

50. Maze I, Shen L, Zhang B, Garcia BA, Shao N, Mitchell A, et al. Analytical tools and current challenges in the modern era of neuroepigenomics. Nat Neurosci. 2014;17:1476–90.

51. Kennedy BC, Wallin DJ, Tran PV, Georgieff MK. Long-term brain and behavioral consequences of early-life iron deficiency. Fetal Development: Research on Brain and Behavior, Environmental Influences, and Emerging Technologies; 2016. p. 295–316.

52. Cusick SE, Barks A, Georgieff MK. Nutrition and brain development. Curr Top Behav Neurosci. 2022;53:131–65.

53. Liao R, Zheng Y, Liu X, Zhang Y, Seim G, Tanimura N, et al. Discovering how Heme controls genome function through Heme-omics. Cell Rep. 2020;31:107832.

54. Singh G, Segura BJ, Georgieff MK, Gisslen T. Fetal inflammation induces acute immune tolerance in the neonatal rat hippocampus. J Neuroinflammation. 2021;18.

55. Szepesi Z, Manouchehrian O, Bachiller S, Deierborg T. Bidirectional microglia–neuron communication in health and disease. Front Cell Neurosci. 2018;323.

56. Zeisel S. Choline, other methyl-donors and epigenetics. Nutr. 2017;9:445.

57. Andersen SL. Trajectories of brain development: point of vulnerability or window of opportunity? Neurosci Biobehav Rev. 2003;27:3–18.

58. Barks A, Beeson MM, Hallstrom TC, Georgieff MK, Tran PV. Developmental Iron deficiency dysregulates TET activity and DNA Hydroxymethylation in the rat Hippocampus and cerebellum. Dev Neurosci. 2022;44:80–90.

59. Le Merre P, Esmaeili V, Charrière E, Galan K, Salin PA, Petersen CCH, et al. Reward-based learning drives rapid sensory signals in medial prefrontal cortex and dorsal Hippocampus necessary for goal-directed behavior. Neuron. 2018;97:83-91.e5.

60. LeGates TA, Kvarta MD, Tooley JR, Francis TC, Lobo MK, Creed MC, et al. Reward behaviour is regulated by the strength of hippocampus–nucleus accumbens synapses. Nat. 2018;564:258–62.

61. Tang J, Dani JA. Dopamine enables in vivo synaptic plasticity associated with the addictive drug nicotine. Neuron. 2009;63:673–82.

62. Márquez J, Campos-Sandoval JA, Peñalver A, Matés JM, Segura JA, Blanco E, et al. Glutamate and Brain Glutaminases in Drug Addiction. Neurochem Res. 2016;42:846–57.

63. Enoch M-A, Zhou Z, Kimura M, Mash DC, Yuan Q, Goldman D. GABAergic gene expression in postmortem Hippocampus from alcoholics and cocaine addicts; corresponding findings in alcohol-Naïve P and NP rats. PLoS One. 2012;7:e29369.

64. Castilla-Ortega E, Serrano A, Blanco E, Araos P, Suárez J, Pavón FJ, et al. A place for the hippocampus in the cocaine addiction circuit: potential roles for adult hippocampal neurogenesis. Neurosci Biobehav Rev. 2016;66:15–32.

65. Takahashi Y, Valencia MM, Yu Y, Ouchi Y, Takahashi K, Shokhirev MN, Lande K, Williams AE, Fresia C, Kurita M, et al. Transgenerational inheritance of acquired epigenetic signatures at CpG islands in mice. Cell. 2023;186(4):715-+.

66. Datta M, Staszewski O, Raschi E, Frosch M, Hagemeyer N, Tay TL, Blank T, Kreutzfeldt M, Merkler D, Ziegler-Waldkirch S, et al. Histone deacetylases 1 and 2 regulate microglia function during development, homeostasis, and neurodegeneration in a context-dependent manner. Immunity. 2018;48(3):514-+.

67. Erny D, Dokalis N, Mezö C, Castoldi A, Mossad O, Staszewski O, Frosch M, Villa M, Fuchs V, Mayer A, et al. Microbiota-derived acetate enables the metabolic fitness of the brain innate immune system during health and disease. Cell Metab. 2021;33(11):2260-+.

68. Farrelly LA, Thompson RE, Zhao S, Lepack AE, Lyu Y, Bhanu NV, Zhang BC, Loh YHE, Ramakrishnan A, Vadodaria KC, et al. Histone serotonylation

Liu *et al. BMC Genomics*   (2024) 25:301

Page 17 of 17

is a permissive modification that enhances TFIID binding to H3K4me3. Nature. 2019;567(7749):535-+.

69. Sperber H, Mathieu J, Wang YL, Ferreccio A, Hesson J, Xu ZJ, Fischer KA, Devi A, Detraux D, Gu HW, et al. The metabolome regulates the epigenetic landscape during naive-to-primed human embryonic stem cell transition. Nat Cell Biol. 2015;17(12):1523–35.

70. Wei JB, Yu XB, Yang L, Liu XL, Gao BY, Huang BX, Dou XY, Liu J, Zou ZY, Cui XL, et al. FTO mediates LINE1 m6A demethylation and chromatin regulation in mESCs and mouse development. Science. 2022;376(6596):968-+.

71. Tran PV, Fretham SJB, Wobken J, Miller BS, Georgieff MK. Gestationalneonatal iron deficiency suppresses and iron treatment reactivates IGF signaling in developing rat hippocampus. Am J Physiol - Endocrinol Metab. 2012;302:316–24.

72. Petry CD, Eaton MA, Wobken JD, Mills MM, Johnson DE, Georgieff MK. Iron deficiency of liver, heart, and brain in newborn infants of diabetic mothers. J Pediatr. 1992;121:109–14.

73. Wong-Goodrich SJE, Glenn MJ, Mellott TJ, Blusztajn JK, Meck WH, Williams CL. Spatial memory and hippocampal plasticity are differentially sensitive to the availability of choline in adulthood as a function of choline supply in utero. Brain Res. 2008;1237:153–66.

74. Glenn MJ, Kirby ED, Gibson EM, Wong-Goodrich SJ, Mellott TJ, Blusztajn JK, et al. Age-related declines in exploratory behavior and markers of hippocampal plasticity are attenuated by prenatal choline supplementation in rats. Brain Res. 2008;1237:110–23.

75. Schmidt AT, Alvarez GC, Grove WM, Rao R, Georgieff MK. Early iron deficiency enhances stimulus-response learning of adult rats in the context of competing spatial information. Dev Cogn Neurosci. 2012;2:174–80.

76. Corces MR, Trevino AE, Hamilton EG, Greenside PG, Sinnott-Armstrong NA, Vesuna S, et al. An improved ATAC-seq protocol reduces background and enables interrogation of frozen tissues. Nat Methods. 2017;14:959–62.

77. Tran PV, Kennedy BC, Lien Y-C, Simmons RA, Georgieff MK. Fetal iron deficiency induces chromatin remodeling at the Bdnf locus in adult rat hippocampus. Am J Physiol Integr Comp Physiol. 2015;308:R276–82.

78. Buenrostro J, Wu B, Chang H, Greenleaf W. ATAC-seq: a method for assaying chromatin accessibility genome-wide. Curr Protoc Mol Biol. 2015;109:21.29.1.

79. Kim D, Paggi JM, Park C, Bennett C, Salzberg SL. Graph-based genome alignment and genotyping with HISAT2 andHISAT-genotype. Nat Biotechnol. 2019;37:907.

80. Zhang Y, Liu T, Meyer CA, Eeckhoute J, Johnson DS, Bernstein BE, et al. Model-based Analysis of ChIP-Seq (MACS). Genome Biol. 2008;9:1–9.

81. Shen L, Shao N-Y, Liu X, Maze I, Feng J, Nestler EJ. diffReps: detecting differential chromatin modification sites from ChIP-seq data with biological replicates. PLoS One. 2013;8:e65598.

82. Quinlan AR, Hall IM. BEDTools: a flexible suite of utilities for comparing genomic features. Bioinformatics. 2010;26:841–2.

83. Heinz S, Benner C, Spann N, Bertolino E, Lin YC, Laslo P, et al. Simple combinations of lineage-determining transcription factors prime cisregulatory elements required for macrophage and B cell identities. Mol Cell. 2010;38:576–89.

84. Liao Y, Smyth GK, Shi W. featureCounts: an efficient general purpose program for assigning sequence reads to genomic features. Bioinformatics. 2014;30:923–30.

85. Robinson MD, McCarthy DJ, Smyth GK. edgeR: a Bioconductor package for differential expression analysis of digital gene expression data. Bioinformatics. 2010;26:139–40.

Publisher's Note